Kinetic analysis of complex solid state reactions.

A new deconvolution procedure

Antonio Perejón, Pedro. E. Sánchez-Jiménez, José M. Criado and Luis A. Pérez-Maqueda[*]

Instituto de Ciencia de Materiales de Sevilla. C. Américo Vespucio 49, Sevilla 41092. Spain

EMAIL ADDRESS: maqueda@cica.es

RUNNING TITLE: Kinetic analysis of complex solid state reactions

[*]Corresponding author . Tel +34954489548 Fax +34954460665

1

Kinetic analysis of complex solid state reactions.

A new deconvolution procedure

ABSTRACT

The kinetic analysis of complex solid state reactions that involve simultaneous overlapping processes is challenging. A method that involves the deconvolution of the individual processes from the overall differential kinetic curves obtained under linear heating rate conditions, followed by the kinetic analysis of the discrete processes using combined kinetic analysis is proposed. Different conventional mathematical fitting functions have been tested for deconvolution, paying special attention to the shape analysis of the kinetic curves. It has been shown than many conventional mathematical curves such as the Gaussian and Lorentzian ones fit inaccurately kinetic curves and the subsequent kinetic analysis yields incorrect kinetic parameters. Alternatively, other fitting functions such as the Fraser-Suzuki one properly fits the kinetic curves independently of the kinetic model followed by the reaction and their kinetic parameters, moreover the subsequent kinetic analysis yields the correct kinetic parameters. The method has been tested with the kinetic analysis of complex processes both simulated and experimental.

KEYWORDS: Kinetic Analysis, solid-state reactions, deconvolution, complex processes.

1. Introduction

Solid state reactions are in many cases complex and involve several overlapping processes. The kinetic analysis of such solid state reactions is challenging, as far as the kinetic parameters, i.e. activation energy, preexponential factor and kinetic model, of each individual process should be determined for a complete kinetic description of the overall reaction. Thus, while a large number of analytical methods are available for determining the kinetic parameters of discrete solid state reactions, the number of procedures for the analysis of complex processes is much more limited. Methods for the analysis of discrete processes include isoconversional or model-free methods,[1-3] model fitting procedures,[4] master plots,[5-7] non parametric analysis,[8,9] and combined kinetic analysis.[10,11] For complex processes, non linear regression methods are the most commonly used.[12-14] In general, a reaction scheme with different processes is assumed, while the kinetic parameters, i.e activation energy and preexponential factor, corresponding to the different individual processes are optimized by an iterative procedure that minimizes an objective function, usually defined as a function of the difference between the experimental curves and the curves reconstructed using the kinetic parameters to be optimized.

An interesting alternative for the kinetic analysis of complex processes with overlapping reactions implies separating the individual processes by peak deconvolution, using statistical functions, followed by the kinetic analysis of the separated peaks to calculate the kinetic parameters. Different deconvolution functions have been used in literature, being the Lorentz distribution function one of the most extensively used. Examples of solid state reactions where this latter function is used for the separation of the individual processes include the thermal decomposition of poly[B-(methylamino)borazine] precursor into boron nitride,[15] the thermal decomposition of a polymer made from silsesquioxanes that convert into silicon oxycarbide ceramics on pyrolysis,[16] the thermal decomposition of hydromagnesite that involves different decomposition steps, i.e. dehydration, dehydroxylation and decarbonation,[17] the thermal degradation of cellulose derivatives/starch blends,[18]

and the pyrolysis reactions in industrial waste activated sludge.[19] Wagner et al have proposed the use of Gaussian functions for the deconvolution of the overlapping processes in the differential scanning calorimetry traces corresponding to the crystallization of chalcogenide glasses.[20] Other statistical functions such as the Weibull and logistic mixture models have been also used for fitting complex solid state reactions, such as thermal degradation of polyurethane, [21,22] wheat straw oxidative pyrolysis,[23] and animal bones combustion.[24]

The objective of the present paper is performing a comparative study of the different deconvolution functions for fitting curves corresponding to the diverse kinetic models proposed in literature for solid state reactions, including a shape analysis of the kinetic curves. Additionally, a new procedure for performing the kinetic analysis of complex solid state reactions will be proposed. The method involves the deconvolution of the differential curves obtained at different linear heating rates followed by the combined kinetic analysis of the resulting individual curves to obtain the kinetic parameters without assumptions about the kinetic model followed by the reaction. This procedure will be tested with both simulated and experimental curves.

2. Theoretical

The reaction rate for a single solid state process in conditions far from equilibrium is described by two functions, one of the reaction temperature and another of the extent of conversion, i.e. *k(T)* and *f(α)*, respectively:

$$\frac{d\alpha}{dt} = k(T)f(\alpha) \tag{1}$$

being α the reaction fraction, *t* the time and *T* the temperature. In general, *k(T)* is described by an Arrhenius expression:

$$k(T) = Ae^{-E/RT} \tag{2}$$

4

where A is the Arrhernius preexponential factor, E is the activation energy, and R is the gas constant. For $f(\alpha)$, a number of expressions have been proposed in literature, a selection of the most common ones are included in Table 1. These latter expressions have been proposed considering different physical ideal models that take into consideration certain geometrical and driving forces for solid state processes.[25,26] A complete kinetic analysis procedure involves the calculation of both $k(T)$ and $f(\alpha)$ functions that properly describe the solid state process.

2.1 Determination of the activation energy from isoconversional methods

The activation energy, E, as a function of the reacted fraction can be determined from isoconversional methods without any previous assumption on the kinetic model fitted by the reaction. One of the most extensively used isoconversional method is that proposed by Friedman[1] that provides accurate values of activation energies even if they were function of the reacted fraction.[27]

Taking into consideration the Arrhenius expression (eq 2), the general kinetic equation (eq 1) can be written in logarithmic form as follows:

$$ln\left(\frac{d\alpha}{dt}\right) = ln(Af(\alpha)) - \frac{E}{RT} \tag{3}$$

At a constant value of α, $f(\alpha)$ would be also constant and eq 3 would be written in the form:

$$ln\left(\frac{d\alpha}{dt}\right)_\alpha = Const - \frac{E_\alpha}{RT_\alpha} \tag{4}$$

Thus, the activation energy at a constant α value, E_α, can be determined from the slope of the plot of the left hand side of eq 4, that is the logarithm of the reaction rate at a constant value of α, versus the inverse of the temperature at the same value of α.

5

2.2 Combined kinetic analysis

The combined kinetic analysis allows determining the kinetic triplet (E, A, and f(α)) from the simultaneous analysis of a set of different curves measured under any different temperature programs (not necessarily linear).[10,11,28] In this method, the kinetic model is determined in the following general form:

$$f(\alpha) = c(1 - \alpha)^n \alpha^m \qquad (5).$$

This equation can accurately fit every ideal kinetic model included in Table 1 by adjusting the parameters c, n and m. Besides, this equation (eq 5) can also describe deviations of the ideal kinetic models due to inhomogeneities in the shape and size of the solid particles.[10] By introducing eq 5 into eq 3 and rearranging terms it follows

$$\ln\left(\frac{d\alpha}{dt}\right) - \ln((1 - \alpha)^n \alpha^m) = \ln(cA) - \frac{E}{RT} \qquad (6).$$

This latter equation is the basic equation for the combined kinetic analysis. Thus, the experimental sets of data, i.e. α, $d\alpha/dt$, and T, corresponding to several temperature programs are substituted into eq 6, while the parameters n and m that provide the best linearity (maximum coefficient of linear correlation, r) to the plot of the left hand side of eq 6 versus the reciprocal temperature, are determined by an optimization procedure. Thus, the entire set of experimental data is used for the determination of the n and m parameters. Once the values of n and m that maximize r are found, the values of E and $\ln(cA)$ are estimated respectively from the slope and intercept of the linear plot. Finally, the kinetic model is discriminated by comparing the shape of the f(α) function resulting from the optimization procedure with that of the functions corresponding to the ideal kinetic models included in Table 1.

2.3 Deconvolution

Different fitting functions have been used for the deconvolution process, namely:

Gaussian:

$$y = a_0 exp\left[-\frac{1}{2}\left(\frac{x-a_1}{a_2}\right)^2\right]$$ (7),

where a0, a1, and a2 are amplitude, center, and width of the curve, respectively;

Lorentzian:

$$y = \frac{a_0}{1+\left(\frac{x-a_1}{a_2}\right)^2}$$ (8),

where the parameter a0, a1, and a2 have the same meaning as in the Gaussian function.

Weibull:[29]

$$y = a_0 \left(\frac{a_3-1}{a_3}\right)^{\frac{1-a_3}{a_3}} \left(\frac{x-a_1}{a_2} + \left(\frac{a_3-1}{a_3}\right)^{\frac{1}{a_3}}\right)^{a_3-1} exp\left[-\left(\frac{x-a_1}{a_2} + \left(\frac{a_3-1}{a_3}\right)^{\frac{1}{a_3}}\right)^{a_3} + \frac{a_3-1}{a_3}\right]$$ (9),

where a0, a1, a2 and a3 are amplitude, center, width and shape of the curve, respectively;

and Fraser-Suzuki:[30,31]

$$y = a_0 \ exp\left[-ln2\left[\frac{\ln\left(1+2a_3\frac{x-a_1}{a_2}\right)}{a_3}\right]^2\right]$$ (10),

where a0, a1, a2 and a3 are amplitude, position, halfwidth and asymmetry of the curve, respectively.

Two different computer programs were used for nonlinear least squares curve fitting: Peakfit (Systat Software Inc.) and Fityk (distributed under the terms of GNU General Public License). The functions that were not included as standard functions were introduced as user defined functions (Fraser-Suzuki for both programs and Weibull for Fityk). Equivalent results were obtained from both computer programs.

3. Results

A shape analysis of the kinetic curves is of interest for determining the suitability of the different fitting functions used for deconvolution of complex solid-state processes. The value of the reaction fraction, α, at the maximum reaction rate is indicative of the symmetry of the kinetic curve. Thus, this study is detailed here.

Under linear heating rate conditions, the general equation (eq 1) can be written as follows

$$\frac{d\alpha}{dT} = \frac{A}{\beta} e^{-\frac{E}{RT}} f(\alpha) \tag{11},$$

where β is the heating rate. The differentiation of eq 11 yields:

$$\frac{d^2\alpha}{dt^2} = \left(\frac{E\beta}{RT^2} + Af'(\alpha)e^{\frac{-E}{RT}}\right)\left(\frac{d\alpha}{dt}\right) \tag{12}.$$

At the maximum reaction rate, $d^2\alpha/dt^2$ is zero, and therefore:

$$\frac{E\beta}{RT_m^2} = -Af'(\alpha_m)e^{\frac{-E}{RT_m}} \tag{13},$$

where T_m and α_m are the temperature and reacted fraction at the maximum, respectively.

Besides, eq 11 can be integrated yielding

$$g(\alpha) = \frac{AE}{\beta R}\int_x^\infty \frac{e^{-x}}{x^2}dx = \frac{AE}{\beta R}p(x) \tag{14},$$

being $x=E/RT$. From eqs 13 and 14, it follows:

$$\frac{\exp(-x)}{x^2}\frac{1}{p(x)}g(\alpha_m)f'(\alpha_m) + 1 = 0 \tag{15}.$$

Table 2 includes the values of α_m obtained from eq 15, using an 8th degree rational approximation to $p(x)$,[32,33] as a function of x (E/RT), for the different kinetic models in Table 1. It is clear from Table 2

that values of α at the maximum rate are different from 0.5, indicating that kinetic curves are asymmetrical. Therefore, functions such as the Lorentzian or Gaussian ones that yield symmetrical curves seem to be inadequate for fitting kinetic curves, while the Weibull and Fraser-Suzuki functions that allow fitting the asymmetry of the curves might be more adequate. Kinetic curves were simulated by assuming all the different kinetic models in Table 1 and fitted using the Lorentzian, Gaussian, Weibull, and Fraser-Suzuki equations. As a way of example, Figure 1 shows a curve simulated assuming a R2 kinetic model and the resulting fitting curves using Lorentzian, Gaussian, Weibull, and Fraser-Suzuki equations. It is quite clear from Figure 1 that the kinetic curve is asymmetrical and, therefore, the fitting with Lorentzian and Gaussian functions is poor, while Weibull and Fraser-Suzuki equations nicely fit the kinetic curve, being the Fraser-Suzuki equation the one that provides the best fit. Similar results were obtained for the different kinetic models in Table 1. Figure 2 includes a set of four kinetic curves simulated using a fourth order Runge-Kutta numerical integration by assuming three different kinetic models, that is a phase boundary reaction, R3, a nucleation and growth reaction, A2, and a diffusion controlled reaction, D3. These curves were very nicely fitted by the Fraser-Suzuki equation (Figure 2). To further validate the ability of the Fraser-Suzuki equation for fitting kinetic curves that deviate from the ideal kinetic modes due to inhomogeneities in the size of the solid particles, another curve was simulated assuming a D2 kinetic model and a log normal particle size distribution with a standard deviation in logarithmic scale of 0.75.[34,35] Figure 2d shows that this latter kinetic curve was properly fitted by the Fraser-Suzuki equation. Similar results were obtained for other particle size distribution functions and other heterogeneities, such as inhomogeneities in particle shape. Therefore, we can conclude that the Fraser-Suzuki equation can accurately fit kinetic curves obtained not only by assuming ideal kinetic models, but also kinetic curves simulated by assuming deviations of the ideal kinetic models due to inhomogeneities in particle size distribution or particle shape. On the contrary, Lorentzian and Gaussian functions fail to fit asymmetrical curves such as kinetic curves. Therefore, to fit kinetic curves obtained for a single process with a Lorentzian or Gaussian fitting function requires of more than a single fitting function, as shown in Figure 3, where a single simulated curve requires at least

three Gaussian function to get an accurate fit. Thus, a single process would be incorrectly detected as a complex one and, therefore, obtaining kinetic information from this fitting would be meaningless.

Figures 4 and 5 include the same set of simulated linear heating rate kinetic curves fitted with Lorentzian and Fraser-Suzuki equations, respectively. It is clear from these figures (Figures 4 and 5) that the Fraser-Suzuki function provides a much better fitting than the Lorentzian one, as expected from the results discussed above. The activation energy values, as obtained from the isoconversional analysis of the Lorentzian and Fraser-Suzuki curves resulting of the fitting are included in Figure 6. For the Fraser-Suzuki curves, the resulting values of activation energy are coincident with that used in the simulation (180 kJ mol^{-1}) and invariant in the entire α range, as expected from the accurate fitting of the simulated curves. For the Lorentzian curves, only for values of α in the range from 0.1 to 0.5, the calculated activation energy values are coincident with that used in the simulation (180 kJ mol^{-1}), showing significant deviations mostly in the range of large values of α. The combined kinetic analysis plots, that are the values calculated for the left hand side of eq 6 using the n and m parameters obtained from the optimization procedure for the set of Lorentzian (Figure 4) and Fraser-Suzuki (Figure 5) curves versus 1/T, are included in Figures 7a and 8a respectively. In both cases, curves corresponding to the different heating rates are fitted by a single straight line, being the linear correlation for the Fraser-Suzuki curves better than that for the Lorentzian ones. The slopes of the plots lead to activation energy values that are coincident with the expected value for the Fraser-Suzuki curves (180 ± 1 kJ mol^{-1}) and slightly larger for the Lorentzian curves (185 ± 2 kJ mol^{-1}). Figures 7b and 8b show the comparison of the f(α) function resulting from the combined analysis for the Lorentzian and Fraser-Suzuki curves, respectively, with some of the conversion functions often used in the literature (listed in Table 1). It is clear from these figures that the conversion function associated with the Fraser-Suzuki curves (Figure 8b) matches an F1 kinetic model, as that used in the simulation, while the conversion function associated with the Lorentzian curves (Figure 7b) match a diffusion type model. These results indicate that when a suitable function, such as the Fraser-Suzuki function, is used to fit the experimental kinetic

curves, the resulting kinetic parameters and kinetic model are properly determined. In contrast, the use of an inadequate function, such as the Lorentzian one, for fitting the experimental kinetic curves might yield to erroneous results from the kinetic analysis. Similar conclusions were drawn for other fitting equations that yield symmetric curves such as Gaussian, Voigt or Pearson VII that do not fit properly the kinetic curves, but for the sake of brevity the complete analysis has not been reported in detail here.

Figure 9 shows a set of kinetic curves simulated for linear heating rate conditions by assuming two independent processes that take place simultaneously (the kinetic parameters are included in the figure caption). These curves have been fitted with two Fraser-Suzuki functions that very accurately match the simulated curves (Figure 9). Thus, the contribution of each independent process can be deconvoluted and independently analyzed as shown above. The activation energy values, as obtained from the isoconversional analysis of the two deconvoluted processes were 125 ± 4 kJ mol^{-1} and 196 ± 4 kJ mol^{-1}, respectively. These values are coincident with those used in the simulation. The combined kinetic analysis plots for the first and second process are included in Figure 10. The slope of the plots lead to activation energy values of 124 ± 1 kJ mol^{-1} and 195 ± 1 kJ mol^{-1} for the first and second process, respectively. Figure 11 shows the comparison of the f(α) function resulting from the combined analysis for both processes with some of the conversion functions often used in the literature (listed in Table 1). The kinetic models resulting from the analysis are coincident with those used in the simulation, i.e.R3 for the first process and A2 for the second one. These results have shown that in the case of independent overlapping process, the Fraser-Suzuki fitting function can be effectively used to deconvolute the individual processes, while the kinetic parameters can be determined, in a second step, by means of the combined kinetic analysis of the individual curves. Nevertheless, in case of more complex processes, such as in consecutive reactions or when products from one of the processes react with some other reactants or products, the situation would be different to the one described here and further investigation would be required. In fact, we are now working on trying to solve those situations.

To test the proposed method with experimental curves, the thermal dehydrochlorination of PVC has been chosen as a model reaction. This reaction has been extensively studied in literature with a very broad dispersion of published results, but recently, it has been shown that PVC dehydrochlorination is complex and involves two simultaneous independent processes.[26,36-38] These two processes could be related with the presence of two chlorine groups with different tacticities.[26,38-41] From the kinetic point of view the overall reaction rate can be formulated as follows:[26]

$$\frac{d\alpha}{dt} = l_1 A_1 \exp\left(\frac{-E_1}{RT}\right) f_1(\alpha_1) + l_2 A_2 \exp\left(\frac{-E_2}{RT}\right) f_2(\alpha_2) \qquad (16),$$

where the subscripts 1 and 2 refer to the first and second process, respectively, l_1 and l_2 being the contribution fraction of the first and second process to the overall reaction. It is evident that l_1 and l_2 must accomplish the following relationships:

$$l_1 + l_2 = 1 \qquad (17)$$

$$l_1 \alpha_1 + l_2 \alpha_2 = \alpha \qquad (18)$$

Figure 12 includes a set of experimental thermogravimetric curves in its differential form for the thermal dehydrochlorination of about 10 mg of PVC sample (Aldrich 389323: average Mn ~47,000; average Mw ~80,000, fine powder) under different linear heating rate conditions and in flow of nitrogen (100 cm^3 min^{-1}). For these experiments, a homemade thermogravimetric instrument has been used.[36,37] The curves have been very accurately fitted with two Fraser-Suzuki functions, as shown in Figure 12. Once the contribution of each individual process was deconvoluted, each one was independently analyzed. The isoconversional analysis yielded activation energy values, that remained constant for the entire α range studied (0.1-0.9), of 111 ± 6 kJ mol^{-1} and 202 ± 7 kJ mol^{-1} for the first and second processes, respectively. The combined kinetic analysis plots for the first and second process are included in Figure 13. The slope of the plots lead to activation energy values of 111 ± 1 kJ mol^{-1} and 202 ± 2 kJ mol^{-1} for the first and second process, respectively, while the intercept yields to values of cA of 2.2 (± 0.4) 10^{10} min^{-1} and 7.2 (±0.8)·10^{16} min^{-1} for the first and second process, respectively. Figure

14 shows the comparison of the f(α) function resulting from the combined analysis for both processes with some of the conversion functions often used in the literature (listed in Table 1). The kinetic models resulting from the analysis were for the first process an A2 (Random instant nucleation and two-dimensional growth of nuclei) model and for the second one a diffusion controlled (closed to the three-dimensional diffusion, Jander equation, D3) model. Both the kinetic models and the kinetic parameters obtained for both process of the PVC dehydrochlorination are in agreement with those previously reported by us.[26] Using these kinetic parameters, it was possible to reconstruct the experimental curves. Thus, Figure 15 shows, as a way of example, the overlay of the experimental curve obtained at 10 K min^{-1} and the curve simulated assuming this heating rate and the kinetic parameters obtained from the analysis, showing an excellent match.

4. Conclusions

The use of deconvolution for discriminating among individual processes in complex solid state reactions has been explored. It has been shown that conventional functions such as the Lorentzian and Gaussian ones, which are commonly used in literature for deconvoluting complex solid state reactions, are inadequate due to the fact that kinetic curves are asymmetrical, whereas the Fraser-Suzuki algorithm, that allows to accommodate asymmetric functions, fits properly any kinetic curve whatever would be the kinetic model obeyed by the solid state reaction. In fact, it has been shown that Fraser-Suzuki function is able to fit not only kinetic curves that follow ideal kinetic models but even reactions whose kinetic model deviates from the ideal ones due to inhomogeneities in particle size or shape. Based on these results a new kinetic analysis procedure for obtaining the kinetic parameters for complex solid state reactions has been proposed. The method involves the deconvolution of the complex reaction into its individual processes, using the Fraser-Suzuki function, followed by the kinetic analysis of the individual processes using a combined kinetic analysis. This latter method allows determining the entire kinetic triplet without any assumption about the kinetic model or the values of the kinetic parameters.

The deconvolution method here proposed has been successfully tested with kinetic curves simulated assuming overlapping independent solid state reactions. Furthermore, it has been also tested with experimental data, in particular with the thermal dehydrochlorination of PVC that takes place through a mechanism that involves two independent processes; thus, parameters of all both overlapping reactions have been determined.

Acknowledgement

References.

(1)   Friedman, H. L. *J. Polym. Sci. Polym. Symp.* **1964**, 183.
(2)   Vyazovkin, S. Isoconversional Kinetics. In *Handbook of thermal analysis and calorimetry*; Brown, M. E., Gallagher, P., Eds.; Elsevier: Amsterdam, The Netherlands, 2008.
(3)   Ozawa, T. *Bull. Chem. Soc. Jpn.* **1965**, *38*, 1881.
(4)   Khawam, A.; Flanagan, D. R. *J. Phys. Chem. B* **2005**, *109*, 10073.
(5)   Gotor, F. J.; Criado, J. M.; Malek, J.; Koga, N. *J. Phys. Chem. A* **2000**, *104*, 10777.
(6)   Sanchez-Jimenez, P. E.; Perez-Maqueda, L. A.; Perejon, A.; Criado, J. M. *J. Phys. Chem. A* **2010**, *114*, 7868.
(7)   Criado, J. M.; Perez-Maqueda, L. A.; Gotor, F. J.; Malek, J.; Koga, N. *J. Therm. Anal. Calorim.* **2003**, *72*, 901.
(8)   Sempere, J.; Nomen, R.; Serra, R.; Soravilla, J. *Thermochim. Acta* **2002**, *388*, 407.
(9)   Sempere, J.; Nomen, R.; Serra, R. *J. Therm. Anal. Calorim.* **1999**, *56*, 843.
(10)   Sanchez-Jimenez, P. E.; Perez-Maqueda, L. A.; Perejon, A.; Criado, J. M. *Polym. Degrad. Stab.* **2009**, *94*, 2079.
(11)   Perez-Maqueda, L. A.; Criado, J. M.; Malek, J. *J. Non-Cryst. Solids* **2003**, *320*, 84.
(12)   Marcilla, A.; Beltrán, M. *Polym. Degrad. Stab.* **1995**, *48*, 219.
(13)   Opfermann, J. *J. Therm. Anal. Calorim.* **2000**, *60*, 641.
(14)   Font, R.; Conesa, J. A.; Molto, J.; Munoz, M. *J. Anal. Appl. Pyrolysis* **2009**, *85*, 276.
(15)   Bernard, S.; Fiaty, K.; Cornu, D.; Miele, P.; Laurent, P. *J. Phys. Chem. B* **2006**, *110*, 9048.
(16)   Soraru, G. D.; Pederiva, L.; Latournerie, M.; Raj, R. *J. Am. Ceram. Soc.* **2002**, *85*, 2181.
(17)   Koga, N.; Yamane, Y. *J. Therm. Anal. Calorim.* **2008**, *93*, 963.
(18)   Alvarez, V. A.; Vazquez, A. *Polym. Degrad. Stab.* **2004**, *84*, 13.
(19)   Yang, X. Y.; Jiang, Z. P. *Bioresour. Technol.* **2009**, *100*, 3663.
(20)   Wagner, C.; Vazquez, J.; Villares, P.; Jimenezgaray, R. *Mater. Lett.* **1994**, *18*, 280.
(21)   Barbadillo, F.; Fuentes, A.; Naya, S.; Cao, R.; Mier, J. L.; Artiaga, R. *J. Therm. Anal. Calorim.* **2007**, *87*, 223.

(22)   Cai, J. M.; Liu, R. *J. Phys. Chem. B* **2007**, *111*, 10681.

(23)   Cai, J. M.; Alimujiang, S. *Ind. Eng. Chem. Res.* **2009**, *48*, 619.

(24)   Jankovic, B.; Adnadevic, B.; Kolar-Anic, L.; Smiciklas, I. *Thermochim. Acta* **2010**, *505*, 98.

(25)   Khawam, A.; Flanagan, D. R. *J. Phys. Chem. B* **2006**, *110*, 17315.

(26)   Sanchez-Jimenez, P. E.; Perez-Maqueda, L. A.; Perejon, A.; Criado, J. M. *Polym. Degrad. Stab.* **2010**, *95*, 733.

(27)   Criado, J. M.; Sanchez-Jimenez, P. E.; Perez-Maqueda, L. A. *J. Therm. Anal. Cal.* **2008**, *92*, 199.

(28)   Perez-Maqueda, L. A.; Criado, J. M.; Gotor, F. J.; Malek, J. *J. Phys. Chem. A* **2002**, *106*, 2862.

(29)   Weibull, W. *J. Appl. Mech.* **1951**, *18*, 293.

(30)   Fraser, R. D. B.; Suzuki, E. *Anal. Chem.* **1966**, *38*, 1770.

(31)   Fraser, R. D. B.; Suzuki, E. *Anal. Chem.* **1969**, *41*, 37.

(32)   Perez-Maqueda, L. A.; Criado, J. M. *J. Therm. Anal. Calorim.* **2000**, *60*, 909.

(33)   Perez-Maqueda, L. A.; Sanchez-Jimenez, P. E.; Criado, J. M. *Int. J. Chem. Kinet.* **2005**, *37*, 658.

(34)   Perez-Maqueda, L. A.; Criado, J. M.; Sanchez-Jimenez, P. E. *J. Phys. Chem. A* **2006**, *110*, 12456.

(35)   Koga, N.; Criado, J. M. *J. Am. Ceram. Soc.* **1998**, *81*, 2901.

(36)   Criado, J. M.; Perez-Maqueda, L. A.; Dianez, M. J.; Sanchez-Jimenez, P. E. *J. Therm. Anal. Calorim.* **2007**, *87*, 297.

(37)   Dianez, M. J.; Perez-Maqueda, L. A.; Criado, J. M. *Rev. Sci. Instrum.* **2004**, *75*, 2620.

(38)   Gonzalez, N.; Mugica, A.; Fernandez-Berridi, M. J. *Polym. Degrad. Stab.* **2006**, *91*, 629.

(39)   Rogestedt, M.; Hjertberg, T. *Macromolecules* **1993**, *26*, 60.

(40)   Millan, J. L.; Martinez, G.; GomezElvira, J. M.; Guarrotxena, N.; Tiemblo, P. *Polymer* **1996**, *37*, 219.

(41)   Guarrotxena, N. On the secondary molecular structures dependences of physical behaviour of polymers. 2. Application to thermal relaxation, aging and basic electrical poperties of poly(vinylchloride) (PVC) and polypropylene In *International Perspectives on Chemistry and Biochemical Research*; Zaikov, G., Lobo, V., Guarrotxena, N., Eds.; Nova Science Publisher: Hauppauge, NY, USA, 2003; pp 15.

TABLE 1. f(α) and f'(α), i.e. df(α)/dα, kinetic functions for the most widely used kinetic models, including the newly proposed random scission model.

Mechanism	Symbol	f(α)	f'(α)	g(α)
Phase boundary controlled reaction (contracting area)	R2	$(1-\alpha)^{1/2}$	$\dfrac{-1}{2(1-\alpha)^{1/2}}$	$2\left[1-(1-\alpha)^{1/2}\right]$
Phase boundary controlled reaction (contracting volume)	R3	$(1-\alpha)^{2/3}$	$\dfrac{-2}{3(1-\alpha)^{1/3}}$	$3\left[1-(1-\alpha)^{1/3}\right]$
Random nucleation followed by an Instantaneous growth of nuclei. (Avrami-Erofeev eqn. $n=1$)	F1	$(1-\alpha)$	-1	$-\ln(1-\alpha)$
Random nucleation and growth of nuclei through different nucleation and nucleus growth models. (Avrami-Erofeev eqn $\neq 1$.)	An	$n((1-\alpha)[-\ln(1-\alpha)]^{1-1/n}$	$\dfrac{n\ln(1-\alpha)+n-1}{[-\ln(1-\alpha)]^{1/n}}$	$[-\ln(1-\alpha)]^{1/n}$
Two-dimensional diffusion	D2	$(1-\alpha)\ln(1-\alpha)+\alpha$	$\dfrac{-1}{(1-\alpha)[\ln(1-\alpha)]^2}$	$(1-\alpha)\ln(1-\alpha)+\alpha$
Three-dimensional diffusion (Jander equation)	D3	$\dfrac{3(1-\alpha)^{2/3}}{2[1-(1-\alpha)^{1/3}]}$	$\dfrac{1/2-(1-\alpha)^{-1/3}}{[1-(1-\alpha)^{1/3}]^2}$	$\left[1-(1-\alpha)^{1/3}\right]^2$
Three-dimensional diffusion (Ginstling-Brounshtein equation)	D4	$\dfrac{3}{2\left[(1-\alpha)^{-1/3}-1\right]}$	$\dfrac{-(1-\alpha)^{-4/3}}{2[(1-\alpha)^{-1/3}-1]^2}$	$(1-2\alpha/3)-(1-\alpha)^{2/3}$
Random Scission of polymer chain L=2	L2	$2(\alpha^{1/2}-\alpha)$	$\dfrac{1}{\alpha^{1/2}}-2$	$-2\ln(\alpha^{1/2}-1)$

TABLE 2. Values of α_m as obtained from eq. (15) for the different kinetic models included in Table 1 as a function of x (E/RT).

Model	x			
	10	20	50	100
R2	0.7058	0.7266	0.7403	0.7451
R3	0.6521	0.6762	0.6922	0.6979
F1	0.5699	0.5985	0.618	0.6249
A2	0.6022	0.6157	0.6251	0.6285
A3	0.6124	0.6212	0.6275	0.6297
D2	0.7528	0.7947	0.8184	0.826
D3	0.5878	0.6452	0.6801	0.6919
D4	0.6801	0.7287	0.757	0.7664
L2	0.5323	0.5511	0.5644	0.5693

Figure Captions

Figure 1. Overlay of the simulated curve (dots; E = 200 kJ mol^{-1}; A =6 10^{17}min^{-1}, R2 kinetic model, and linear heating rate conditions, 10 K min^{-1}) and the Gaussian (a), Lorentzian (b), Weibull (c) and Fraser-Suzuki (d) curves (solid lines) used for fitting the simulated curve. Residuals are plotted underneath the plots. Correlation coefficients have been included into the figure.

Figure 2. Overlay of the simulated curves (dots) assuming different kinetic parameters (a) R3, E = 150 kJ mol^{-1}, A = 1.2·10^{15} min^{-1}, and β = 5 K min^{-1}; (b) A2, E = 150 kJ mol^{-1}, A = 6·10^{13} min^{-1}, and β=2.5 K min^{-1}; (c) D3, E = 120 kJ mol^{-1}, A = 6·10^{7} min^{-1}, and β = 1 K min^{-1}; (d) D2 with a log normal particle size distribution (0.75), E = 100 kJ mol^{-1}, A = 10^{5} min^{-1}, and β = 10 K min^{-1}, and the Fraser-Suzuki function used for fitting the simulated curves (solid lines). Residuals are plotted underneath the figures. Correlation coefficients have been included into the figure.

Figure 3. Simulated kinetic curve (dots, A2, E = 150 kJ mol^{-1}, A =6 10^{13} min^{-1}, and β = 2.5 K min^{-1}) fitted with three Gaussian function (solid lines).

Figure 4. Overlay of the simulated kinetic curves (dots, F1, E = 180 kJ mol^{-1} and A =6·10^{11} min^{-1}) assuming different linear heating rates: (a) 1 K min^{-1}, (b) 2.5 K min^{-1}, (c) 5 K min^{-1} and (d) 10 K min^{-1}, and the Lorentzian function (solid lines) used for fitting the simulated curves. Residuals are plotted underneath the figures. Correlation coefficients have been included into the figure.

Figure 5. Overlay of the simulated kinetic curves (dots, F1, E = 180 kJ mol^{-1} and A =6·10^{11} min^{-1}) at different linear heating rates: (a) 1 K min^{-1}, (b) 2.5 K min^{-1}, (c) 5 K min^{-1} and (d) 10 K min^{-1}, and the Fraser-Suzuki function (solid lines) used for fitting the simulated curves. Residuals are plotted underneath the figures. Correlation coefficients have been included into the figure.

Figure 6. Activation energy values as a function of α, as obtained from the isoconversional analysis of the Lorentzian and Fraser-Suzuki curves resulting of the fitting of kinetic curves shown in Figures 4 and 5.

Figure 7. (a) Combined analysis plot for Lorentzian curves resulting of the fitting of kinetic curves in Figure 4. (b) Comparison of the f(α) functions (lines) normalized at α= 0.5 [f(α)/f(0.5)] corresponding to some of the ideal kinetic models included in Table 1 with the f(α) function with the resulting values of n and m coefficients, i.e., n= 1.684 and m= 0.056 (dots).

Figure 8. (a) Combined analysis plot for Fraser-Suzuki curves resulting of the fitting of kinetic curves in Figure 5. (b) Comparison of the f(α) functions (lines) normalized at α= 0.5 [f(α)/f(0.5)] corresponding to some of the ide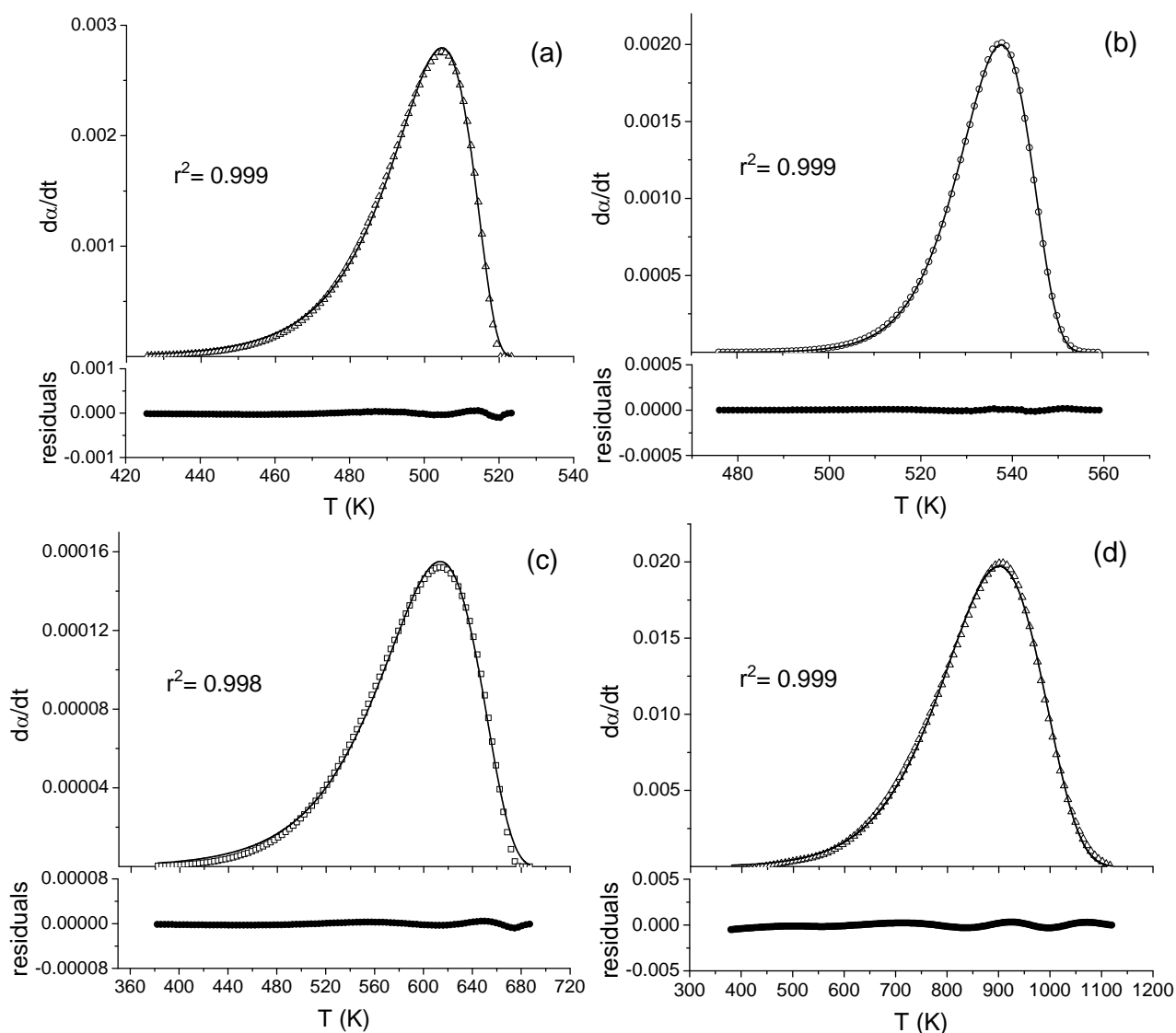al kinetic models included in Table 1 with the f(α) function with the resulting values of n and m coefficients, i.e., n= 0.996 and m= 0.00117 (dots).

Figure 9. Overal of kinetic curves (dots) simulated by assuming two independent processes (f1(α) = R3; E1 = 125 kJ mol^{-1}; A1 = 10^8 min^{-1}; Contribution: 30% and f2(α) = A2; E2 = 195 kJ mol^{-1}; A1 = $2 \cdot 10^{12}$ min^{-1}; Contribution: 70%) at different linear heating rates: (a) 1 K min^{-1}, (b) 2.5 K min^{-1}, (c) 5 K min^{-1} y (d) 10 K min^{-1}, and the two Fraser-Suzuki functions whose overlapping fit the experimental curves (solid lines). Residuals and correlation coefficients are shown.

Figure 10. Combined analysis plot for Fraser-Suzuki curves resulting of the fitting of kinetic curves in Figure 9: (a) first and (b) second process.

Figure 11. Comparison of the f(α) functions (lines) normalized at α= 0.5 [f(α)/f(0.5)] corresponding to some of the ideal kinetic models included in Table 1 with the f(α) function resulting of the combined analysis (dots) for the first (a) and second (b) process in Figure 9.

Figure 12. Overlay of experimental thermogravimetric curves in its differential form for the thermal dehydrochlorination of PVC (dots) at different linear heating rates: (a) 2.5 K min^{-1}, (b) 5 K min^{-1}, (c) 10

K min^{-1} and (d) 15 K min^{-1}, and the corresponding Fraser-Suzuki function used for fitting the experimental curves (solid lines). Residuals are plotted underneath the figures. Correlation coefficients have been included into the figure.
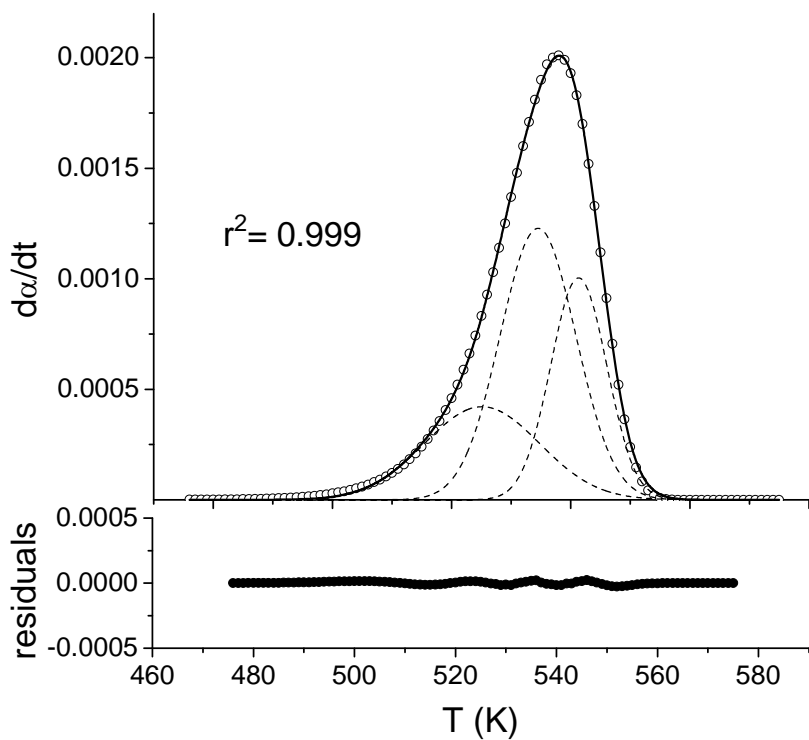
Figure 13. Combined analysis plot for Fraser-Suzuki curves resulting of the fitting of experimental curves in Figure 12: (a) first and (b) second process.

Figure 14. Comparison of the f(α) functions (lines) normalized at α= 0.5 [f(α)/f(0.5)] corresponding to some of the ideal kinetic models included in Table 1 with the f(α) function resulting of the combined analysis (dots) for the first (a) and second (b) process in Figure 12.

Figure 15. Experimental curve in its integral and differential forms corresponding to the dehydrochlorination of PVC obtained at 10 K min^{-1} (dots). Reconstructed curves using the kinetic parameters resulting of the combined kinetic analysis are plotted as solid lines.

Figure 1. Overlay of the simulated curve (dots; E = 200 kJ mol^{-1}; A =6 10^{17}min^{-1}, R2 kinetic model, and linear heating rate conditions, 10 K min^{-1}) and the Gaussian (a), Lorentzian (b), Weibull (c) and Fraser-Suzuki (d) curves (solid lines) used for fitting the simulated curve. Residuals are plotted underneath the plots. Correlation coefficients have been included into the figure.

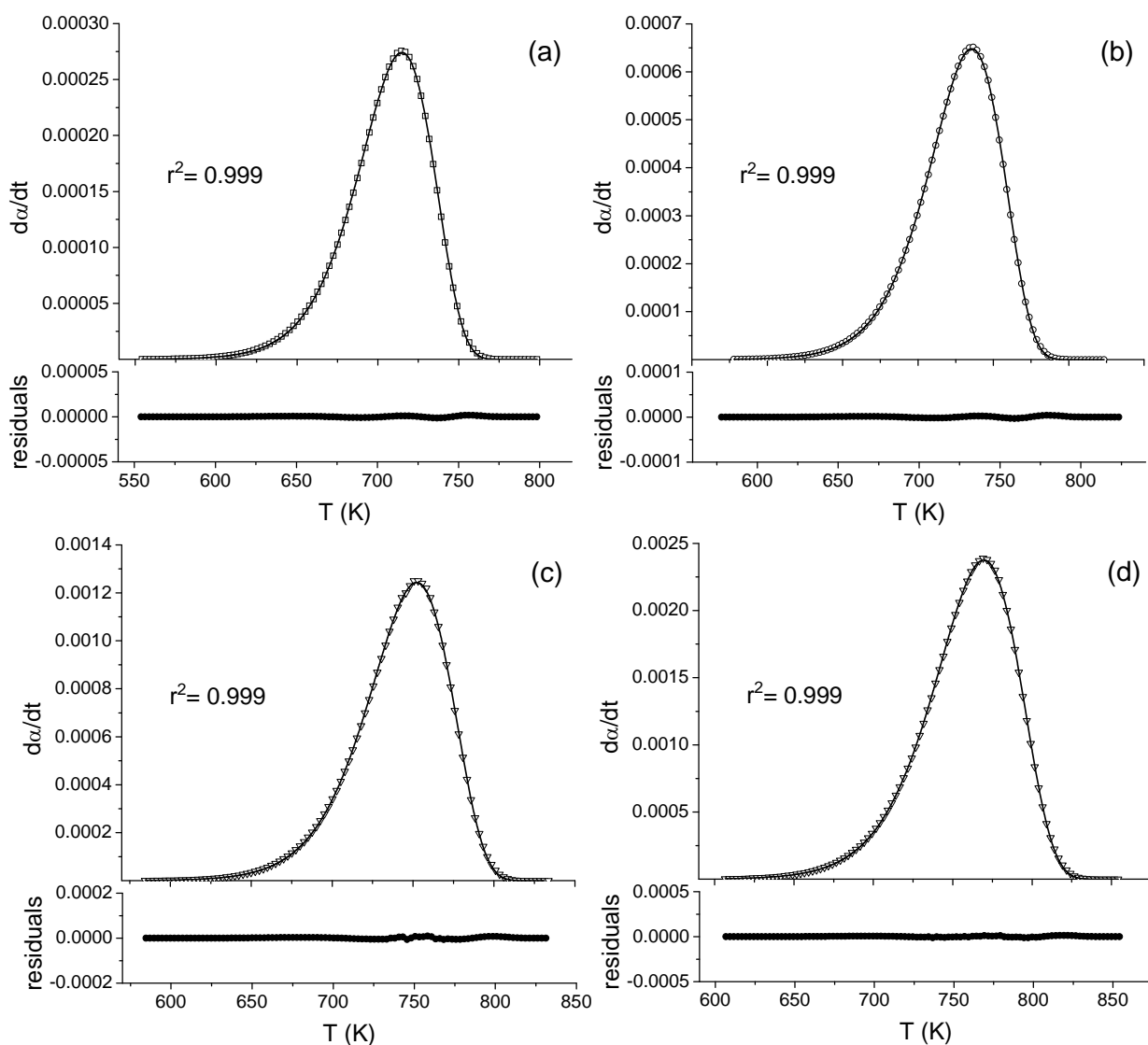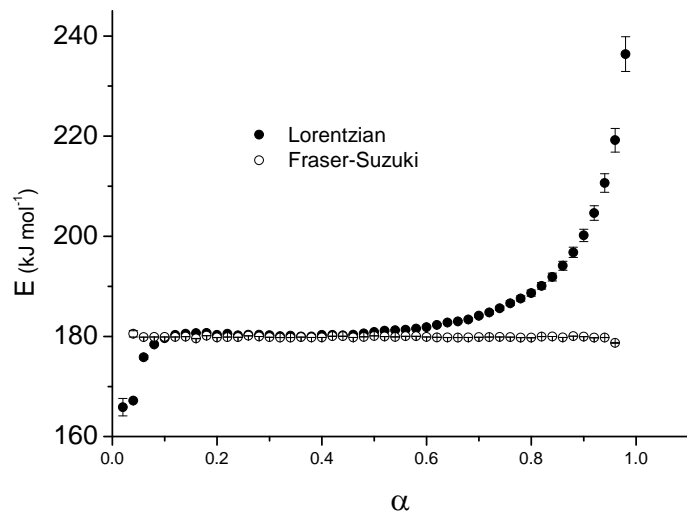**Figure 2.** Overlay of the simulated curves (dots) assuming different kinetic parameters (a) R3, E = 150 kJ mol^{-1}, A = 1.2·10^{15} min^{-1}, and β = 5 K min^{-1}; (b) A2, E = 150 kJ mol^{-1}, A = 6·10^{13} min^{-1}, and β=2.5 K min^{-1}; (c) D3, E = 120 kJ mol^{-1}, A = 6·10^{7} min^{-1}, and β = 1 K min^{-1}; (d) D2 with a log normal particle size distribution (0.75), E = 100 kJ mol^{-1}, A = 10^{5} min^{-1}, and β = 10 K min^{-1}, and the Fraser-Suzuki function used for fitting the simulated curves (solid lines). Residuals are plotted underneath the figures. Correlation coefficients have been included into the figure.

Figure 3. Simulated kinetic curve (dots, A2, $E = 150$ kJ mol^{-1}, $A = 6 \cdot 10^{13}$ min^{-1}, and $\beta = 2.5$ K min^{-1}) fitted with three Gaussian function (solid lines).

Figure 4. Overlay of the simulated kinetic curves (dots, F1, $E = 180$ kJ mol^{-1} and A $=6 \cdot 10^{11}$ min^{-1}) assuming different linear heating rates: (a) 1 K min^{-1}, (b) 2.5 K min^{-1}, (c) 5 K min^{-1} and (d) 10 K min^{-1}, and the Lorentzian function (solid lines) used for fitting the simulated curves. Residuals are plotted underneath the figures. Correlation coefficients have been included into the figure.

Figure 5. Overlay of the simulated kinetic curves (dots, F1, $E = 180$ kJ mol^{-1} and $A = 6 \cdot 10^{11}$ min^{-1}) at different linear heating rates: (a) 1 K min^{-1}, (b) 2.5 K min^{-1}, (c) 5 K min^{-1} and (d) 10 K min^{-1}, and the Fraser-Suzuki function (solid lines) used for fitting the simulated curves. Residuals are plotted underneath the figures. Correlation coefficients have been included into the figure.

25

Figure 6. Activation energy values as a function of α, as obtained from the isoconversional analysis of the Lorentzian and Fraser-Suzuki curves resulting of the fitting of kinetic curves shown in Figures 4 and 5.

Figure 7. (a) Combined analysis plot for Lorentzian curves resulting of the fitting of kinetic curves in Figure 4. (b) Comparison of the f(α) functions (lines) normalized at α= 0.5 [f(α)/f(0.5)] corresponding to some of the ideal kinetic models included in Table 1 with the f(α) function with the resulting values of n and m coefficients, i.e., n= 1.684 and m=0.056 (dots).
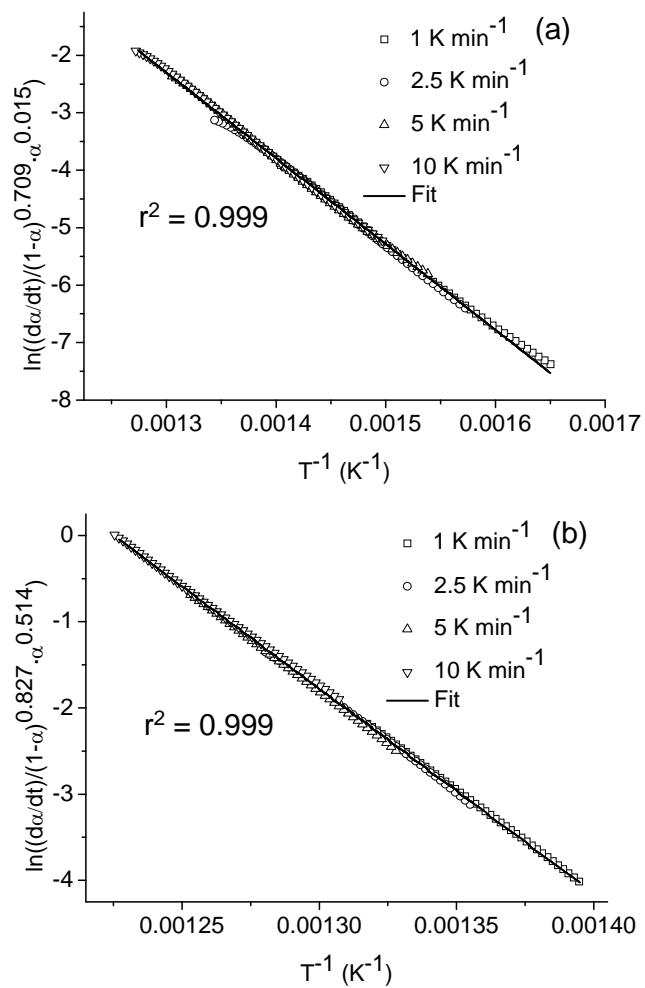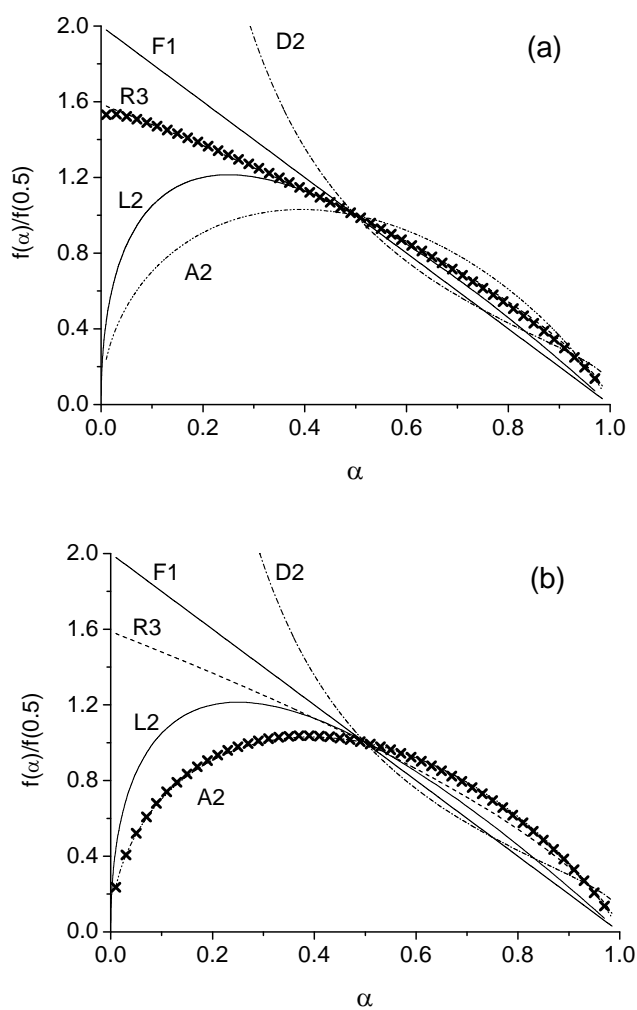
Figure 8. (a) Combined analysis plot for Fraser-Suzuki curves resulting of the fitting of kinetic curves in Figure 5. (b) Comparison of the f(α) functions (lines) normalized at α= 0.5 [f(α)/f(0.5)] corresponding to some of the ideal kinetic models included in Table 1 with the f(α) function with the resulting values of n and m coefficients, i.e., n= 0.996 and m= 0.00117 (dots).

Figure 9. Overal of kinetic curves (dots) simulated by assuming two independent processes ($f1(\alpha)$ = R3; $E1$ = 125 kJ mol^{-1}; $A1$ = 10^8 min^{-1}; Contribution: 30% and $f2(\alpha)$ = A2; $E2$ = 195 kJ mol^{-1}; $A1$ = $2 \cdot 10^{12}$ min^{-1}; Contribution: 70%) at different linear heating rates: (a) 1 K min^{-1}, (b) 2.5 K min^{-1}, (c) 5 K min^{-1} y (d) 10 K min^{-1}, and the two Fraser-Suzuki functions whose overlapping fit the experimental curves (solid lines). Residuals and correlation coefficients are shown.

Figure 10. Combined analysis plot for Fraser-Suzuki curves resulting of the fitting of kinetic curves in Figure 9: (a) first and (b) second process.

Figure 11. Comparison of the f(α) functions (lines) normalized at α= 0.5 [f(α)/f(0.5)] corresponding to some of the ideal kinetic models included in Table 1 with the f(α) function resulting of the combined analysis (dots) for the first (a) and second (b) process in Figure 9.
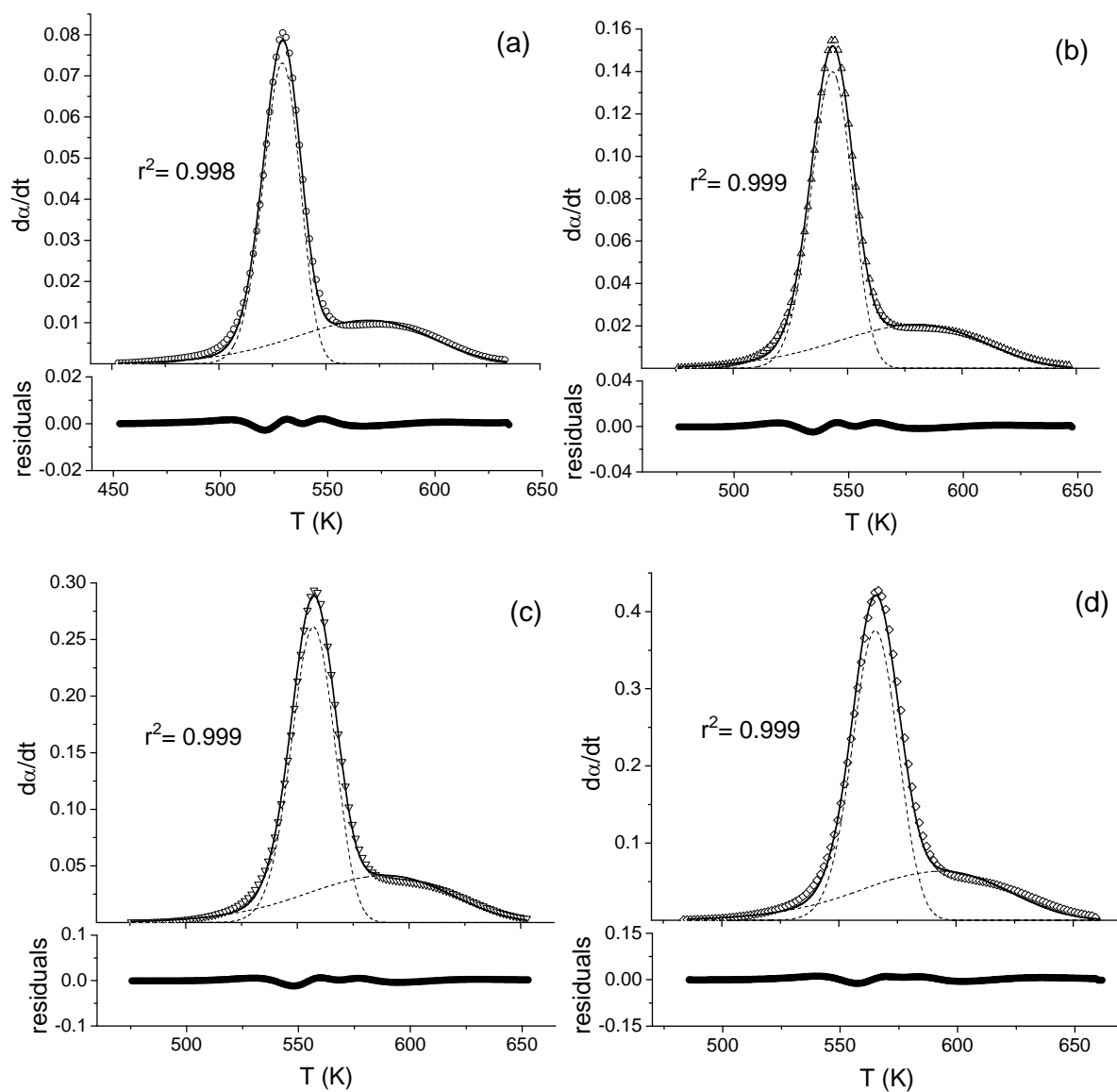
Figure 12. Overlay of experimental thermogravimetric curves in its differential form for the thermal dehydrochlorination of PVC (dots) at different linear heating rates: (a) 2.5 K min^{-1}, (b) 5 K min^{-1}, (c) 10 K min^{-1} and (d) 15 K min^{-1}, and the corresponding Fraser-Suzuki function used for fitting the experimental curves (solid lines). Residuals are plotted underneath the figures. Correlation coefficients have been included into the figure.
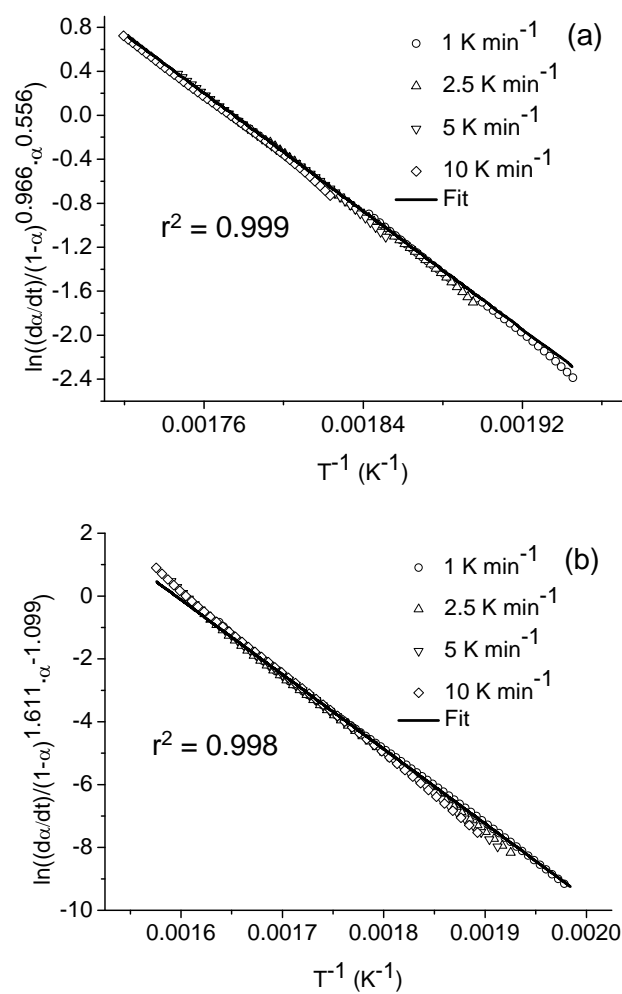
Figure 13. Combined analysis plot for Fraser-Suzuki curves resulting of the fitting of experimental curves in Figure 12: (a) first and (b) second process.
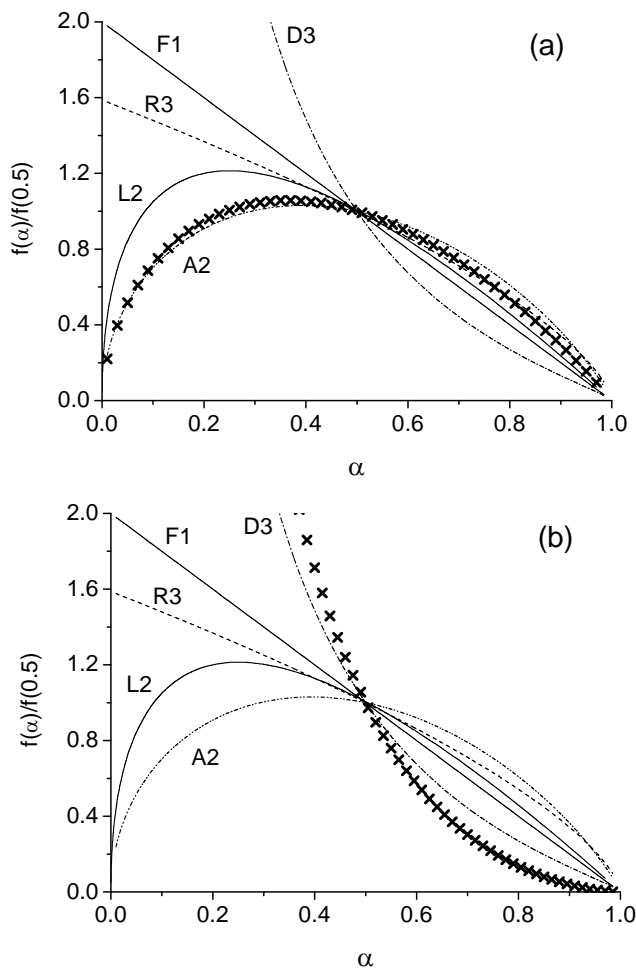
Figure 14. Comparison of the f(α) functions (lines) normalized at α= 0.5 [f(α)/f(0.5)] corresponding to some of the ideal kinetic models included in Table 1 with the f(α) function resulting of the combined analysis (dots) for the first (a) and second (b) process in Figure 12.
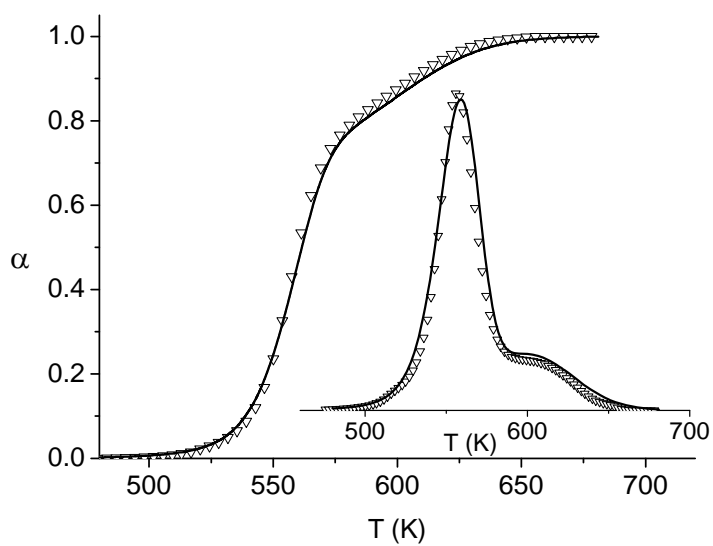
Figure 15. Experimental curve in its integral and differential forms corresponding to the dehydrochlorination of PVC obtained at 10 K min^{-1} (dots). Reconstructed curves using the kinetic parameters resulting of the combined kinetic analysis are plotted as solid lines.

TABLE OF CONTENTS IMAGE